



**HAL**  
open science

## Correlating conductivity and space charge measurements in multi-dielectrics under various electrical and thermal stresses

T.T.N. Vu, G. Teyssedre, Bertrand Vissouvanadin, Séverine Le Roy, Christian Laurent

### ► To cite this version:

T.T.N. Vu, G. Teyssedre, Bertrand Vissouvanadin, Séverine Le Roy, Christian Laurent. Correlating conductivity and space charge measurements in multi-dielectrics under various electrical and thermal stresses. *IEEE Transactions on Dielectrics and Electrical Insulation*, 2015, 22 (1), pp.117-127. 10.1109/TDEI.2014.004507 . hal-03169878

**HAL Id: hal-03169878**

**<https://hal.science/hal-03169878>**

Submitted on 1 Sep 2022

**HAL** is a multi-disciplinary open access archive for the deposit and dissemination of scientific research documents, whether they are published or not. The documents may come from teaching and research institutions in France or abroad, or from public or private research centers.

L'archive ouverte pluridisciplinaire **HAL**, est destinée au dépôt et à la diffusion de documents scientifiques de niveau recherche, publiés ou non, émanant des établissements d'enseignement et de recherche français ou étrangers, des laboratoires publics ou privés.

# Correlating Conductivity and Space Charge Measurements in Multi-dielectrics under Various Electrical and Thermal Stresses

T.T.N. Vu, G. Teyssedre, B. Vissouvanadin, S. Le Roy and C. Laurent

Université de Toulouse; UPS, INPT; LAPLACE (Laboratoire Plasma and Conversion d'Énergie);  
118 route de Narbonne, F-31062 Toulouse cedex 9, France, and CNRS; LAPLACE; F-31062 Toulouse, France

## ABSTRACT

The design of transmission systems requires electric field distribution estimation, which, in case of HVDC application is strongly sensitive to thermal and electrical configuration as well as to the nature of dielectric materials being used owing to the resistive field distribution. In this paper, the field distribution in a dielectric bi-layer of XLPE and rubber materials, as representative of cable junctions, is estimated based on experimental data on field and temperature dependencies of conductivity. Through space charge measurements on bi-layer dielectrics, it is shown that the space charge density and electric field distributions are to a first order estimation consistent with data issued from conductivity measurements. Most notably, the interface charge building up between the two dielectrics changes sign, depending on field and temperature. However, in the high field range (order of 20 kV/mm), charge build-up in the bulk of dielectric materials introduces further distortion to field distribution.

Index Terms-HVDC cable materials, field estimation, interfacial charge.

## 1 INTRODUCTION

WITH a high reliability and a long service life, HVDC transmission systems form the backbone of electric power systems. In a near future polymer insulated HVDC cables might gradually replace oil-impregnated paper insulated HVDC cables owing to the multiples advantages of using synthetic materials. Operating at high temperature, ease of maintenance, mechanical strength, ease assembly of cable joints and environmentally friendly [1]; these properties make polymer dielectrics superior to the actual oil-impregnated paper insulation. An increasing quality of the insulating material for HVDC cable is very important in the development of transmission systems because it influences the breakdown strength of the dielectric.

Pre-molded cable joint which mainly consists of rubber material is commonly used to insure the connection between two High Voltage cable extremities within a long distance transmission system. However, the use of insulating material different from that of the cable leads to the formation of dielectric/dielectric interface in the cable joint. Under DC electric stress, the field distribution in the dielectrics depends on the differences in materials conductivity and permittivity, and the field profile may be quite complex to predict, when considering situations with thermal gradient, non-linear conductivity and divergent geometry as is the case of junctions. In addition, under thermo-electric stresses, space

charge builds up at the interface between dielectrics, as a Maxwell-Wagner effect, and also potentially in the bulk of insulations. These bulk charges produce further redistribution of the electric field. The field intensifications due to these processes may cause accelerated ageing of the insulation system. Although the formation of interfacial charge has been extensively investigated [2, 3] today it is still a major issue for the development of polymeric HVDC cables accessories.

This work aims at investigating interfacial charge and electric field distribution in bi-layer dielectrics intended to HVDC cable system. First, functional variations of conductivity versus electric field and temperature of a rubber material, EPDM, as an example of junction material, and cross-linked polyethylene, XLPE, as cable insulation, have been established based on current-voltage measurements. From there, the polarity of the interfacial charge in XLPE/rubber bi-layer dielectric system has been predicted on the basis of Maxwell-Wagner theory. Furthermore, the density of interfacial charges and the field distribution under various conditions of temperature and field in such a dielectric association have been computed numerically. Finally, space charge measurements have been carried out using the Pulsed Electro-Acoustic, PEA, method in XLPE/rubber bi-layer at different temperatures and fields to check the predicted characteristic of interfacial charge sign and density and to compare with simulation results.

## 2 EXPERIMENTAL SECTION

### 2.1 CONDUCTIVITY MEASUREMENTS

For conductivity measurements, samples are plaques of cross-linked polyethylene (XLPE) or joint material (EPDM, i.e. a cross-linked terpolymer of ethylene, propylene, and diene monomer, containing some mineral charges), referenced as rubber material in the following, with thicknesses varying from 500  $\mu\text{m}$  to 600  $\mu\text{m}$  for each material, and are provided by SilecCable. Samples were kept sealed in aluminum bags after cross-linking.

Gold electrodes of 50 mm diameter were deposited on both faces of samples. To avoid edge phenomena during volt-on measurements, a silicone ribbon was laid at the electrodes periphery. No preliminary heat treatment has been performed on samples so that cross-linking by-products are partially conserved. Measurements were performed in air at different temperatures ranging from 0 to 90  $^{\circ}\text{C}$  by step of 10  $^{\circ}\text{C}$ . The temperature was controlled by a thermo-stated sample holder. For each value of temperature, a new sample has been used for current measurement to avoid possible memory effects. Charging currents (lasting for 1 hour) have been measured for 10 values of DC fields varying between 2 to 25 kV/mm under isothermal condition. Depolarization is applied for 1 hour after each volt-on procedure. Current values were recorded every 2 s during polarization/depolarization procedures.

### 2.2 SPACE CHARGE MEASUREMENTS

The Pulsed Electro-Acoustic (PEA) method was used for measuring space charge distribution in flat bi-dielectric samples (XLPE/rubber). XLPE/rubber bi-layer specimens consist in plaques of about 80 mm in diameter and 500  $\mu\text{m}$  in thickness manufactured by pressing altogether peroxide-containing low density polyethylene and cross-linkable rubber plaques at 180  $^{\circ}\text{C}$  for 15 minutes to complete cross-linking process. Thin gold layers of 20 nm diameter were deposited on each face of samples to form electrodes. XLPE material was connected to the ground and rubber material was connected to DC high voltage. The cycle of polarization/depolarization has been applied to the bi-layer structure. Average electric stress varied between 2 and 30 kV/mm followed by a polarity reversal at -30 kV/mm. Measurement temperatures were 20, 40 and 70 $^{\circ}\text{C}$ . For measurements at 20  $^{\circ}\text{C}$ , the polarization/depolarization steps lasted 3 h/1 h while at 40 and 70  $^{\circ}\text{C}$ , each step lasted 1 hour since shorter duration was required to reach the steady state condition at these temperatures. Space charge profiles were recorded every 100 seconds along the voltage cycle.

### 2.3 CASE OF SPACE CHARGE MEASUREMENT IN MULTIDIELECTRICS

Accumulation of charges at dielectric/dielectric interfaces has been the subject of several studies in recent years using space charge profile measurement techniques. As examples, the effect of interfacial charge in multi-layer oil-paper has been investigated in [4] while space charge build-up in LDPE/EVA has been addressed in [5]. In these studies, it has

been shown that interfacial charge is function of temperature along with the magnitude of applied field.

Since the acoustic properties and dielectric permittivity of materials are specific to the polymeric material investigated, special attention has to be paid regarding space charge recovery in bi-layer dielectrics structures issued from acoustic methods. In the present work using PEA method, the surface charge used for the calibration is first computed using Gauss theorem in addition with the boundary condition on the electric potential assuming that field distribution is purely capacitive: the interfacial charge due to the conductivity mismatch between the two materials can be neglected during the calibration procedure. This assumption holds because the time constant for the build-up of the interfacial charge is of order of tens of minutes (at the highest investigated temperature i.e. 70  $^{\circ}\text{C}$ ) whereas the field is applied for no more than 1 min in the calibration procedure even in worst situations (i.e. in case of noisy signals requiring high number of averaging). Under these considerations, the expression of the surface charge at the ground electrode is given by:

$$\kappa_1 = \frac{\varepsilon_1 \cdot \varepsilon_2 \cdot U}{\varepsilon_2 \cdot d_1 + \varepsilon_1 \cdot d_2} \quad (1)$$

where  $\varepsilon$  and  $d$  are the permittivity and sample thickness and  $U$  is the applied voltage during calibration.

The set-up impulse response  $h_{\text{setup}}(t)$  can be derived from the calibration signal  $v_{\text{PEA1}}$  produced by the surface charge at the ground electrode as follows:

$$h_{\text{setup}}(t) = \frac{1}{\kappa_1} v_{\text{PEA1}}(t) \quad (2)$$

Assuming that acoustic reflection at the interface of the two materials can be neglected, the distribution of charges  $\rho(x)$  at the origin of the raw PEA signal  $v_{\text{PEA}}(t)$  is given by:

$$\rho(t(x)) = \frac{Fe}{v_s(x)} \text{Re} \left[ F^{-1} \left\{ \frac{V_{\text{PEA}}(f)}{H_{\text{setup}}(f)} \right\} \right] \quad (3)$$

where  $V_{\text{PEA}}(f)$  and  $H_{\text{setup}}(f)$  are respectively the Fourier Transforms of the temporal signals  $v_{\text{PEA}}(t)$  and  $h_{\text{setup}}(t)$ .  $Fe$  is the acquisition frequency of the digital oscilloscope and  $v_s(x)$  is the acoustic velocity function in the bi-layer sample being

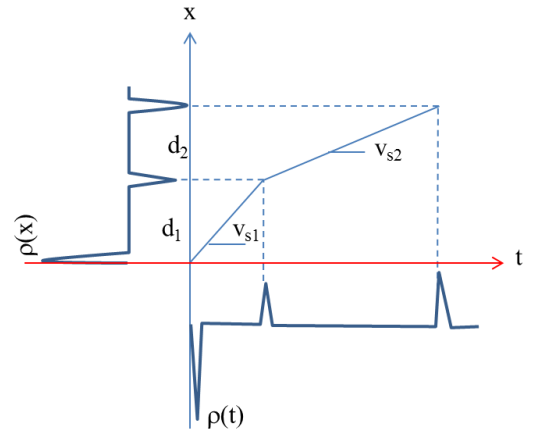


**Figure 1.** Representation of space charge profile versus position from the profile versus time given by the deconvolution of the raw PEA signal in a bi-layer dielectric structure.

$v_{s1}$  and  $v_{s2}$  respectively in the material 1 and material 2.  $F^{-1}$  represents the Inverse Fourier transform operator and  $\text{Re}$  depicts the real part of a complex number. The position  $x$  is related to the time  $t$  (at which the acoustic signal reaches the bottom electrode) through a linear function  $x = v_s * t$ . As shown in Figure 1, a simple homothetic transformation is applied on the time ( $t$ ) to obtain the space charge profile versus position  $\rho(x)$  from the profile versus time  $\rho(t)$  provided by the deconvolution of raw PEA signals.

### 3 CONDUCTION CHARACTERISTICS

#### 3.1 CROSSLINKED POLYETHYLENE

When a DC high voltage is applied to the sample the charging current decreases toward a steady state value, which can be excessively long to reach, depending on stress and temperature. Figure 2 shows the charging current transients in the case of XLPE sample under various applied fields at 30 °C. Charging currents are apparently characterized by two regions: a fast decrease at the beginning of polarization followed by a slower decrease at long time tending to a stable value after about 3000 s (except for high field values –see below) which corresponds to the conduction current.

Overall, when represented in log-log plot (see Figure 2) charging currents are characterized by a quasi-constant slope with time which corresponds to a decrease of the current through an inverse power law with time in the form of  $t^{-n}$  (as an example  $n < 1.3$  for  $T = 30$  °C at any field in the range between 2 and 25 kV/mm). The higher the electric stress the faster the charging current reaches the steady state. For example at 30 °C, under 16 kV/mm, the current value is stabilized after about 90 s while at 6 kV/mm one has to wait for at least 1000 s before reaching the steady state (Figure 2). This is a consequence of the decrease of the relative contribution of the transient current to the total current with increasing field. The increase of the conduction current with the field is non-linear: at 30 °C, the conduction current increases by four decades when the applied field increases by only one decade. For high field levels ( $\geq 19$  kV/mm) one can also notice an increase of the current at long time, which might result from space charge build up in the material.

In addition, an increase of the temperature implies a shorter time to reach the steady state condition (about 1 h at 30 °C and 100 s at 80 °C under 2 kV/mm). Since the resistivity  $\rho(T)$  of the material decreases with temperature, the time constant  $\tau(T) = \rho(T) * \epsilon$  ( $\epsilon$  being the material permittivity) required to reach the steady state condition also decreases with temperature. Figure 3 shows experimental results of conduction current density vs. electric field (J-E) at different temperatures for XLPE. Conduction current values were taken after 1 h of polarization. In the figure, the regression lines to the data at low and high fields are also shown. Even though the charging current is still decreasing after 1 h of polarization for the lowest applied field, it is significantly higher than the current measured at the end of the 1h discharging step at each field level. In all instances, after 1h, the discharge current represents less than 10% of the charging current. So polarization phenomena, if any, represent only a weak

contribution to the current data used to estimate material conductivity.

Following literature reports [6] the intersection of the fitting lines can define a threshold field between two regimes: low field and high field regimes. The value of the threshold field decreases with temperature, being 10 kV/mm, 7.5 kV/mm and 5.5 kV/mm respectively at 20, 30 and 40 °C. With decreasing trend of the threshold field, we can extrapolate this value to about 3.6 kV/mm at 50 °C. No threshold was detected at 70 °C in the investigated field range. This means that the threshold at 70 °C is to be expected below 2 kV/mm. A non-linear behavior is revealed below the threshold field in Figure 3 (the slope is about 1.4 at 20 °C). Such feature may occur when carrier mobility is field-dependent without accumulation of space charge. The decrease in the threshold field is likely to indicate an increase in charge injection rate with temperature. So, space charge accumulation occurs at lower value of field as temperature increases. The dependence of current density with electric field is more pronounced at high field. This behavior is often attributed to space-charge-limited-current (SCLC) mechanism in the case of polyethylene materials [7].

#### 3.2 RUBBER MATERIAL

Charging currents at 30 °C obtained under various electric fields are shown in Figure 4. The transient charging currents for rubber at a temperature of 30 °C (Figure 4) do not stabilize after one hour of polarization, contrary to the case of XLPE material. For example, at 30 °C under 25 kV/mm after 1 h of polarization the current is still decreasing in the case of rubber while for the same condition, the steady state is reached after only 60 s of polarization in the case of XLPE. It must be stressed that although marked current transients are measured, the charging current after 1 h or polarization is, like for XLPE, at least one order of magnitude larger than the discharging current after 1 h, which means that there is no significant overestimation of conductivity due to dipolar effects.

Figure 5 presents the conduction current density vs. electric field of rubber material at different temperatures ranging from 30 to 70 °C. Two conduction regimes are observed as for XLPE material. However, the slopes in the low and high field regimes are lower indicating a weaker variation of the current density with the applied field. It is worth noticing that the threshold field (transition field between the two regimes) appears less temperature dependent than for XLPE (10 kV/mm at 30 and 40 °C; 9 and 7.3 kV/mm respectively at 60 and 70 °C). Below the threshold field, the current-field characteristics follow a sub-linear regime (slopes are of the order of 0.5). Sub-linear conduction with a slope of  $\approx 0.6$  in the J-E curve in the low field regime has been reported for XLPE having undergone substantial outgassing [8, 9]. Measurements were reported for a single temperature and the sub-linear character was not commented. Still in XLPE, Bodega [2] reported a linear or super-linear behavior in the low field regime with a slope in the range 1 to 1.4 for temperatures in the range 20 to 60 °C. In fact, there are not so many reports in the literature where sub-linear conduction phenomena are discussed [10].

In the context of liquid dielectrics, the switch from an

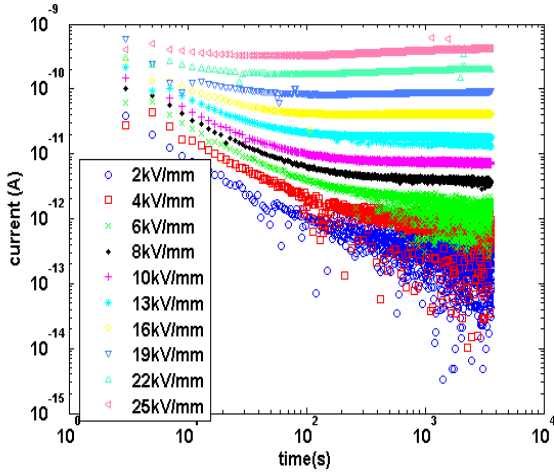


Figure 2. Current vs. time transients for XLPE in log-log scale for different fields at 30 °C.

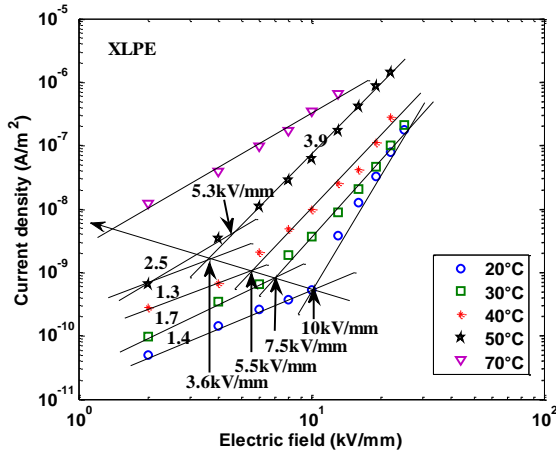


Figure 3. Current density vs. field characteristics for XLPE in log-log scale at different temperatures.

ohmic behavior at low fields to an intermediate sub-linear field regime is explained by the saturation of ionic dissociation rate in the case of pure ionic conduction, or by an electrochemical equilibrium taking place between injection and extraction of electronic charges at the metal-liquid interface [11]. For the later hypothesis, the charge injection and extraction are in electrochemical equilibrium with the formation/neutralization of ions being effectively transported in the liquid. In this way, it has been demonstrated [11] that the current density reaches a saturation regime in certain range of electric field above the ohmic regime. As EPDM is a rubber-like material, its rheological properties approach those of a liquid of high viscosity and some form of ionic processes might be at play in the sub-linear phenomenon. We are aware that the hypothesis should be further substantiated.

### 3.3 FIELD AND TEMPERATURE DEPENDENCIES OF CONDUCTIVITY

It is worth to mention that for both XLPE and rubber material, the current density and therefore the conductivity exhibit a strong dependence with temperature and electric field. In order to have an analytical expression of the

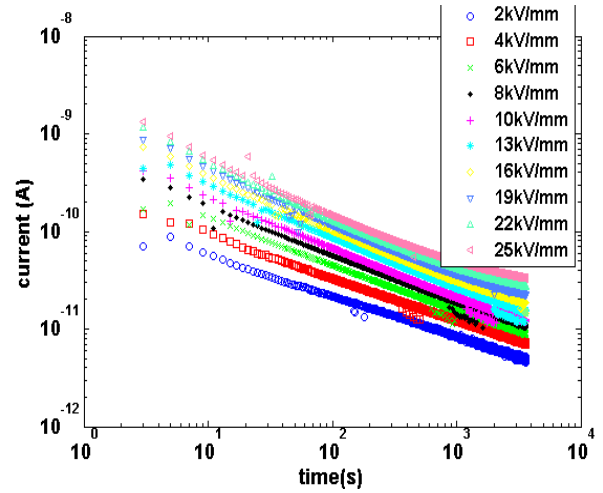


Figure 4. Current vs. time transients for rubber in log-log scale for different fields at 30 °C.

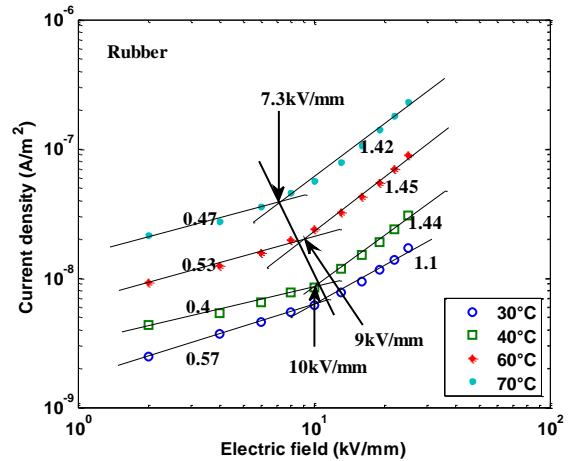


Figure 5. Current density vs. field characteristics for rubber in log-log scale at different temperatures.

conductivity vs. temperature and electric field, a semi-empirical formula, equation (4) has been used to fit the experimental data. Such an approach is usually adopted in literature for this kind of polymer [12-14].

$$\sigma(T, E) = A \cdot \exp\left(\frac{-E_a}{k_B T}\right) \cdot \sinh(B(T) \cdot E) \cdot E^\alpha$$

where

$A$  and  $\alpha$  are constants;

$E_a$  : thermal activation energy;

$k_B$  : Boltzmann's constant ;

$T$  : temperature;

$E$  : applied electric field;

$B = aT + b$  is a temperature-dependent parameter to account for the change in threshold field versus temperature.

Figure 6 presents the experimental current vs. field values already discussed in the previous section, and the fitted current vs. field curves obtained with equation (4), for XLPE (Figure 6a) and rubber material (Figure 6b). Coefficients for XLPE and rubber-based material used for the curve fitting procedure are reported in Table 1. The fitted data are in good agreement with the experimental ones, for all values of fields and

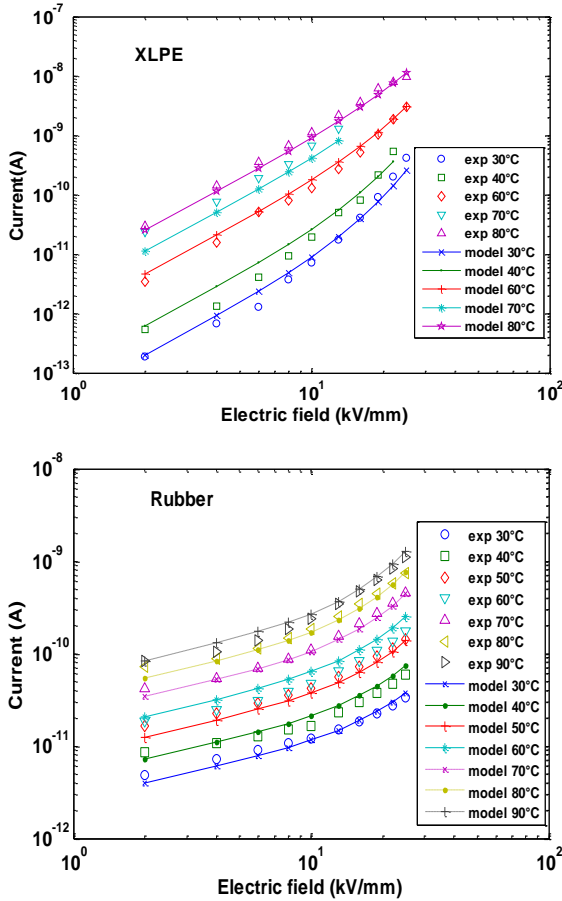


**Figure 6.** Experimental and fitted current vs. field characteristics for (a) XLPE and (b) rubber at different temperatures.

temperatures, and for both materials. Formulas derived from current measurements are subsequently used in our numerical simulation to compute the electric field distribution within a XLPE/ rubber bi-layer structure. It is noticeable in Figure 6 that the conduction current is lower in XLPE than in the rubber at low field, whatever the temperature is. However, at high field the conductivity is higher in XLPE, all the more that the temperature is higher. As will be shown later on, these features have strong consequences on the field distribution depending on temperature / average field.

## 4 SPACE CHARGE IN MULTI-DIELECTRICS

### 4.1 PREDICTED INTERFACIAL CHARGE

The interface charge that builds up between two dielectrics of different nature is treated using Maxwell-Wagner (MW) theory. We consider the situation depicted in Figure 7 where the two materials have different dielectric permittivity, and different conductivity. The field is supposed homogeneous in the layers. Under steady state conditions, the following rules must hold:

- Conservation of the current density, i.e.:

$$\sigma_1(E_1) \cdot E_1 = \sigma_2(E_2) \cdot E_2 \quad (5)$$

- Gauss law:

$$\oiint_S \vec{D} \cdot d\vec{S} = \sum Q_{\text{int}} \quad (6)$$

where  $Q_{\text{int}}$  is the charge stored in the volume limited by the closed surface  $S$ . For the present configuration, it leads to a continuity condition on the dielectric displacement normal to the surface of the form:

$$\varepsilon_1 E_1 = \varepsilon_2 E_2 + \sum_s \quad (7)$$

where  $\varepsilon$  is the dielectric permittivity and  $\sum_s$  is the interfacial charge.

- Boundary condition on the potential:

$$d_1 E_1 + d_2 E_2 = -V_{\text{app}} \quad (8)$$

$V_{\text{app}}$  is the applied voltage,  $d$  is the material thickness. Subscripts 1 and 2 refer to XLPE and rubber respectively (see Figure 7).

The set of equations (5), (7) and (8) has been solved taking into account the field dependency of conductivity obtained in section 3.3. Also, it was supposed that the two layers have the same thickness. Setting fixed the applied voltage, the field values are determined by the combination of equation (5) and (8). Then the interfacial charge can be determined from equation (7). The Comsol® software was used for resolution as the set of equations is non-linear.

From measured conductivity values, using Maxwell-Wagner (MW) theory, we can predict the quantity of interfacial charge as a function of applied voltage and temperature in a bi-layer XLPE/rubber dielectric subjected to DC electric field as depicted in Figure 7.

Figure 8 shows a map of the sign of the calculated interfacial charge in steady state condition as a function of the temperature and average applied field. A temperature and field-dependent demarcation line separates two distinct regions of positive and negative charge at the interface of two dielectrics for temperatures ranging from 0 to 80 °C and for fields between 2 to 25 kV/mm. Space charge measurements presented in the next section will be used to test the capability of this conductivity model issued from conduction measurements in predicting the sign of the interface charge.

**Table 1.** Coefficients for XLPE and EPDM in conductivity Equation (4), with conductivity in S/m, field in V/m, T in K.

	XLPE	Rubber
<b>A</b>	0.8	97
<b><math>E_a</math>(eV)</b>	1	0.44
<b>a (m/V/K)</b>	$1.38 \times 10^{-7}$ (T < 313 K); $-1.3 \times 10^{-9}$ (T ≥ 313 K)	$4.8 \times 10^{-10}$
<b>b (m/V)</b>	0 (T < 313 K); $5.45 \times 10^{-7}$ (T ≥ 313 K)	$-5.1 \times 10^{-7}$
<b><math>\alpha</math></b>	0.15	-1.42

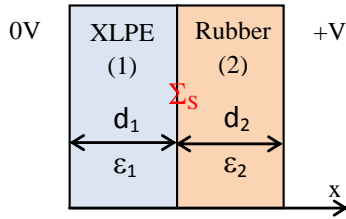


**Figure 7.** XLPE/rubber bi-layer under applied voltage. In both model and measurements, the electrode on the rubber is at positive polarity. For the model, we suppose identical thicknesses,  $d_1=d_2$ . The sign of the interface charge is discussed for the above configuration.

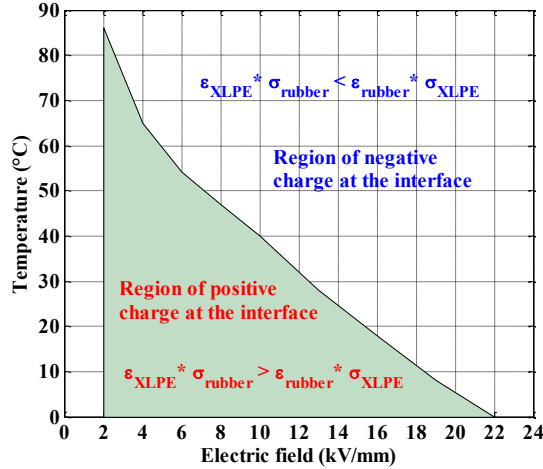


**Figure 8.** Predicted landscape for the sign of the interfacial charge for the configuration represented in Figure 7. The X axis corresponds to the average applied field, i.e.  $V_{app}/(d_1+d_2)$ .

### 4.3 RESULTS FOR XLPE/RUBBER INTERFACE

#### 4.3.1 SIGN OF INTERFACE CHARGE

To check the sign of accumulated charge at the interface calculated in the previous section, space charge measurements have been performed on XLPE-rubber bi-layer flat specimens at three different temperatures 20, 40 and 70 °C for fields in the range of 2 to 30 kV/mm. Specimens were processed targeting the same thickness for XLPE and rubber layers. Figure 9 shows the cartography of space charge density in XLPE/rubber bi-dielectric for the different temperatures. The rubber material and XLPE are connected to the high voltage and ground electrodes respectively. The field values in the stress cycle, as represented at the top of the figures are the same for the three temperatures. However at 20 °C the voltage was applied for a longer time (3 h volts-on / 1 h volts-off at 20 °C vs. 1 h volts-on/ 1 h volts-off at 40 and 70 °C) in each step because the interface charge builds up more slowly.

At 20 °C (Figure 9a), the charge in the interface region, defined by dotted lines in the figure, is positive at low fields, up to 10 kV/mm and in the first instants of the step at 15 kV/mm. For higher fields, the interface charge switches to negative. The calculated interfacial charge, at 20 °C (Figure 8), is also positive for fields below 15 kV/mm, and switches to negative for fields above this value. Note that the interfacial charge is predicted for steady-state conditions.

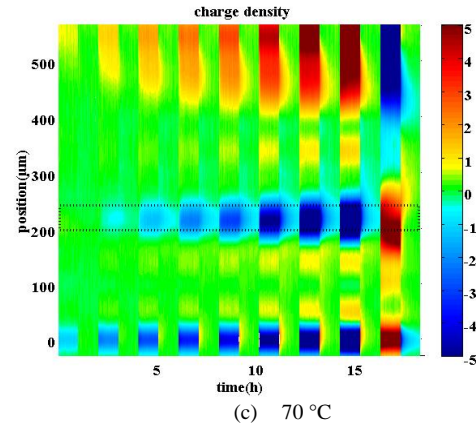
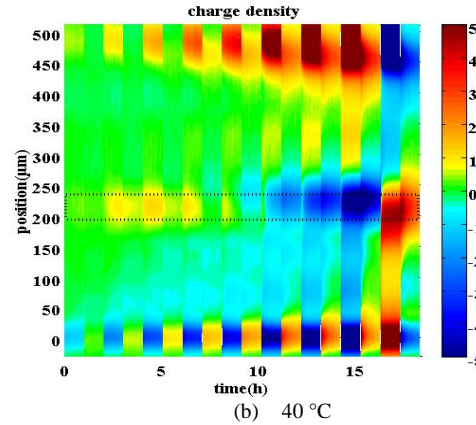
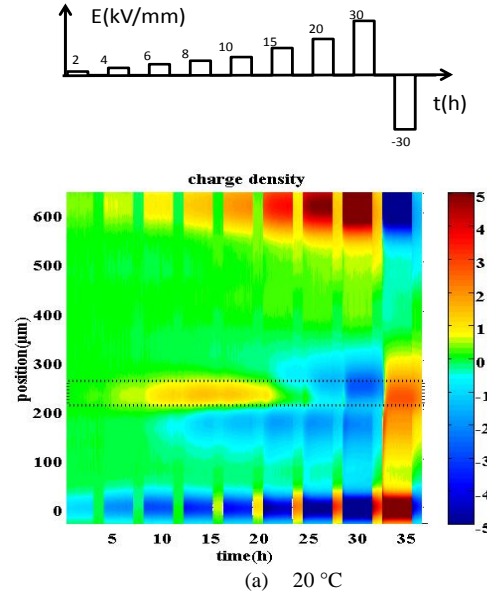


**Figure 9.** Cartography of space charge in XLPE/rubber bi-layer at (a) 20 °C, (b) 40 °C, (c) 70 °C under various electric fields as indicated in the top diagram. Rubber to the top; XLPE to the bottom. Color bar provides charge density scale in  $C/m^3$ .

At 40 °C (Figure 9b), we clearly observe that positive charges accumulate at the interface for applied fields below 10 kV/mm while the development of negative interface charges occurs for fields higher than 15 kV/mm. This change in the charge polarity is due to the change of material conductivity when the field increases. After 1h of polarization at 40 °C, the

interfacial charge is not yet stabilized; for 2 and 4 kV/mm it tends to increase in time while for 10 kV/mm both materials exhibit roughly similar conductivity and the interfacial charge decreases to a negative value. For stresses above 15 kV/mm, the negative interfacial charge is nearly stabilized after 1 h of polarization.

At 70 °C, no evidence of positive interfacial charge has been observed at any field from 2 to 30 kV/mm in the cartography of space charge shown in Figure 9c. Furthermore, the build-up of negative interfacial charges is rapidly achieved (typically within the first 30 min of polarization). The negative polarity of space charge at the interface is consistent with the predicted characteristic of interface charge at 70 °C (see Figure 8). In addition, the maximum value of the predicted interfacial charge under 30 kV/mm is about  $5.9 \times 10^{-4}$  C/m<sup>2</sup> which is higher than that at 20 and 40 °C ( $2 \times 10^{-4}$  C/m<sup>2</sup> at 20 °C and  $3.3 \times 10^{-4}$  C/m<sup>2</sup> at 40 °C). Therefore, not only the polarity of the interfacial charge but also its magnitude is determined by temperature. Furthermore, under polarity reversal to -30 kV/mm (Figure 9), a change in the polarity of the interfacial charge from negative to positive is clearly observed for all temperatures. So, the applied voltage polarity (through the direction of the applied field) also affects the polarity of charges at interfaces along with temperature and the magnitude of the electric stress.

The behavior of these interfacial charges is in agreement with the predicted characteristic of Figure 8. Indeed at 20 and 40 °C, for electric fields less than 15 and 10 kV/mm respectively, positive charges are expected to build-up at the interface while negative charges accumulation is predicted to for higher fields (at 70 °C, negative interfacial charge appears for  $E \geq 4$  kV/mm). In addition to interfacial charges, charges injection occurs at one or both electrodes with a higher density of charges as field is higher.

### 4.3.2 KINETICS OF INTERFACE CHARGE BUILD-UP

Equations (5)-(8) are valid for the steady state condition, i.e. when the interfacial charge is established. The complete set of equations relating the materials properties, interface charge and field distribution in stationary conditions has also been derived for cylindrical geometry by Delpino et al [3]. In non-stationary case, immediately after voltage application, there is no interfacial charge and therefore, the field distribution is controlled by equations (7) and (8). This results in an imbalance of the conduction current in the two materials. Current conservation is restored by introducing a displacement current that is different in the two materials. Still following Maxwell-Wagner theory, the interface charge builds up according to the following rate [15]:

$$\Sigma_s(t) = \frac{\varepsilon_1 \cdot \sigma_2 - \varepsilon_2 \cdot \sigma_1}{\sigma_2 \cdot d_1 + \sigma_1 \cdot d_2} \cdot V_{app} (1 - e^{-t/\tau_{MW}}) \quad (9)$$

where

$$\tau_{MW} = \frac{\varepsilon_2 \cdot d_1 + \varepsilon_1 \cdot d_2}{\sigma_2 \cdot d_1 + \sigma_1 \cdot d_2} \quad (10)$$

The field transient is given by:

$$E_1(t) = \frac{\varepsilon_2 \cdot V_{app} - \Sigma_s(t) \cdot d_2}{\varepsilon_2 \cdot d_1 + \varepsilon_1 \cdot d_2} \quad (11)$$

$$E_2(t) = \frac{\varepsilon_1 \cdot V_{app} - \Sigma_s(t) \cdot d_1}{\varepsilon_2 \cdot d_1 + \varepsilon_1 \cdot d_2} \quad (12)$$

As in the present case the conductivity is field dependent, the field redistribution during interfacial charge build up may lead to situations where the density of interfacial charges diminishes in time or eventually changes sign in the course of charging time under constant applied voltage.

Charge density in experimental profiles has been integrated over the interface region for different levels of applied field:

$$\Sigma_{s\_exp}(t) = \int_{x_1}^{x_2} \rho(x, t) \cdot dx \quad (13)$$

where  $x_1$  and  $x_2$  are defined by the positions in the material shown as dotted lines in Figure 9.

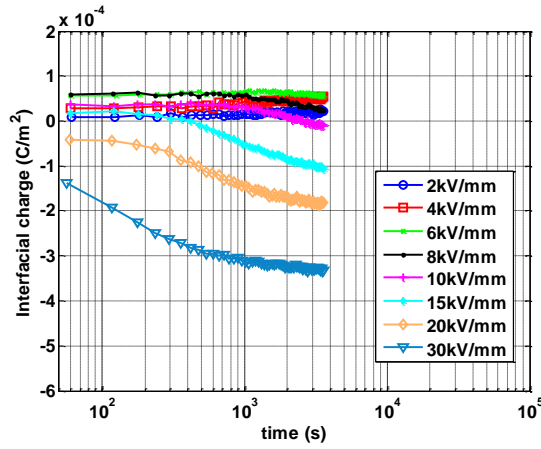
Figure 10 compares the evolution of the experimental (Figure 10a) and simulated (Figure 10b) interfacial charge for different electric stresses at 40 °C. Simulated interfacial charge densities were obtained with exactly the same conditions as in experience. Only the simulation time was extended up to  $10^5$  s to allow studying the dynamic of interfacial charges build-up until the steady state condition. The initial condition ( $t=0$ ) supposes a capacitive field distribution, meaning that the interface charge is null.

For experimental results (Figure 10a), depending on the level of applied electric field, different evolutions in time of interfacial charge density can be observed. The interfacial charge increases slightly in time for fields below 6 kV/mm. In this field range, the interfacial charge obtained after 1 hour of polarization seems to increase with the level of stress. For higher stresses, the interfacial charge diminishes in time and for field strength higher than 10 kV/mm, the sign of the interfacial charge becomes negative after a sufficiently long polarization time.

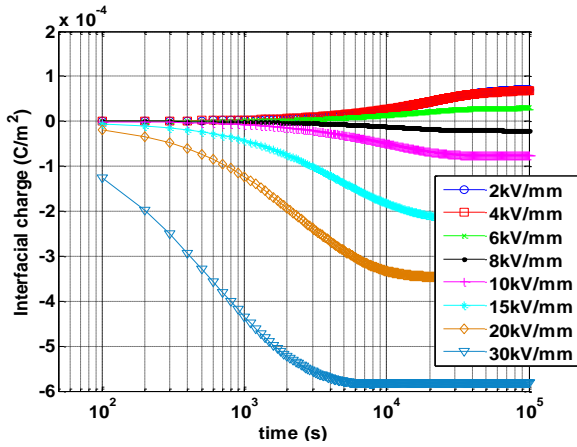
We further notice that the amount of negative interfacial charges increases with the electric stress and the polarization time. The steady state of negative interfacial charges is likely to be reached after 1 hour of polarization only for 30 kV/mm.

Figure 10b shows that for fields lower than 6 kV/mm, the sign of interfacial charges is negative up to several hundred seconds of simulation, and changes from negative to positive afterwards. The steady state is reached after about  $6 \times 10^4$  s (i.e. about 17 hours). For stresses above 8 kV/mm, negative interfacial charges are expected to accumulate. The amount of these negative charges increases with the increasing field. In addition, the kinetic of interfacial charge stabilization is faster for higher electric stress owing to a higher material conductivity. It should be emphasized that in the range of field investigated, the time constant for interfacial charges stabilization is expected to be higher than 1 hour.

The main feature with regard to the dynamic of interfacial charge accumulation can be roughly reproduced by the simulation. However, comparing the amount of interfacial charges taken after 1 hour of polarization, simulation results



(a) Measurement 40 °C



(b) Simulated 40 °C

**Figure 10.** Time dependence of the interfacial charge in XLPE/rubber bi-layer at 40 °C under various mean applied electric fields, i.e.  $V_{app}/(d_1+d_2)$ .

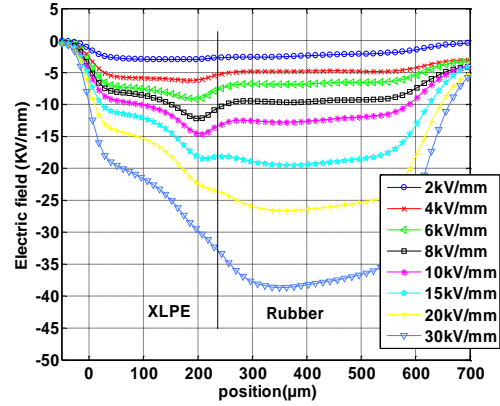
are slightly higher in comparison to the experimental ones. This discrepancy comes probably from the fact that charges injection and trapping mechanisms, which actually occur in the insulation (as observed from space charge patterns), are disregarded in the simulation.

### 4.3.3 FIELD DISTRIBUTION

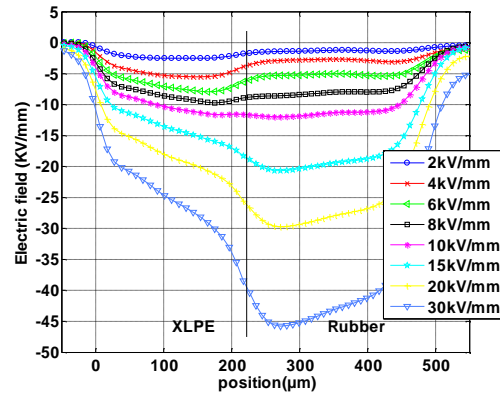
Electric field distributions taken after 3 h for 20 °C, 1 h for 40 and 70 °C under various poling fields are shown in Figure 11. From measurements at 20 °C (Figure 11a) at low field (i.e.  $E \leq 10$  kV/mm), electric field in XLPE is higher than that in the rubber during polarization which is an expected behavior due to a higher conductivity of rubber than XLPE for this condition. It is noticeable that the electric field becomes less homogeneous in XLPE from 6 kV/mm and on: the field is enhanced close to the interface due to the presence of negative charges in the bulk of material. For high stresses ( $E > 10$  kV/mm), since the conductivity of rubber becomes lower than that of XLPE, the highest electric stress is then located in the rubber material. Its maximum value is around 30% greater than the Laplacian field.

Distributions of electric field at 40 and 70 °C in bi-layer XLPE/rubber samples are represented in Figures 11b and 11c respectively, showing the displacement of the position of

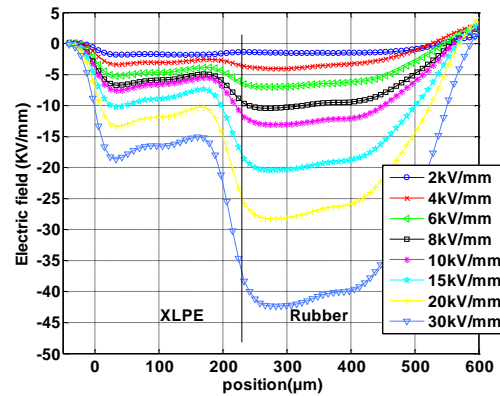
maximum electric stress from one material to the other depending on the magnitude of the applied stress. For applied field lower than 8 kV/mm and 2 kV/mm at 40 and 70 °C respectively, the highest electric stress is located in XLPE material; while for higher electric stresses, the maximum field enhancement is switched into the rubber material. Above the previously mentioned electric stresses, at 40 °C, because of homocharges build-up at both electrodes, the maximum field enhancement is located in the rubber close to the interface. At 70 °C, the apparition of positive heterocharges adjacent to the cathode tends to increase the electric field in XLPE. However the electric stress in the rubber is higher than in XLPE due to a



(a) After 3h at 20 °C



(b) After 1h at 40 °C



(c) After 1h at 70 °C

**Figure 11.** Electric field distribution in XLPE/rubber taken after polarization at (a) 20, (b) 40, (c) 70 °C under various average fields.

much higher quantity of negative charges accumulated at the interface compared to the amount of positive charges in the XLPE material.

Steady state electric field distributions in XLPE/rubber bilayer at 40 °C calculated with equations (5) and (8) are presented in Figure 12 for different average applied fields. The evolution of the electric field in the interface vicinity is in agreement with experimental results. The highest value of the electric field is located in the rubber material for applied fields higher than 10 kV/mm. As previously for interfacial charge prediction, the computed fields are quantitatively different in comparison to experimental results because of the presence of other mechanisms of space charge accumulation, which are not taken into account in the simulation.

## 5 DISCUSSION

The design of cables and accessories for DC applications appears much more complex to achieve compared to AC applications, owing to the poor control and predictability of the field distribution within the insulations. The above results illustrate some of the difficulties faced, such as:

i/ the non-linear dependency of conduction current vs. field, even at moderate fields including design fields for DC cables and accessories, combined to the substantial temperature dependence of conductivity. These features, combined to the fact that these conductivity dependencies with field and temperature vary in an important way from one material to the other lead to very variable field distributions, depending on thermal and electrical stresses. Further features would need to be introduced in real situations; these are the temperature gradient across the accessory due to Joule losses in the conductor, and the coaxial geometry. Though from the modeling standpoint, this does not represent specific difficulty, it may constitute further reasons for important field gradients within accessories. Bodega et al have provided a thorough investigation of interface charge characterization, considering XLPE/EPR interfaces, in flat specimen [16], or cylindrical geometry [3], and with consideration of temperature gradient. Also, the interface charge has been derived for dual dielectric cylindrical geometry [3]. A change in the sign of the interface charge in XLPE/EPR insulations was reported when varying the temperature from 25 to 70 °C [3]. The authors interpreted this behavior as due to negative charge build up in one of the materials that would dominate the interface charge features. However it could be explained as well by the non-linear conductivity in the materials.

ii/ the very slow kinetics to reach equilibrium: interfacial charge build up, and therefore steady state field distribution may take tens of hours to be reached. This may be longer than the variations in current flow through the conductor (linked to fluctuations in energy production/demand), and certainly much longer than the time for voltage reversal that can be applied to cables for inverting the energy flux with thyristor based converters. So, the field distribution, in HVDC cables as well as in accessories, would be permanently out-of-equilibrium, with charges continuously accumulating or redistributing to accommodate cable thermal conditions.

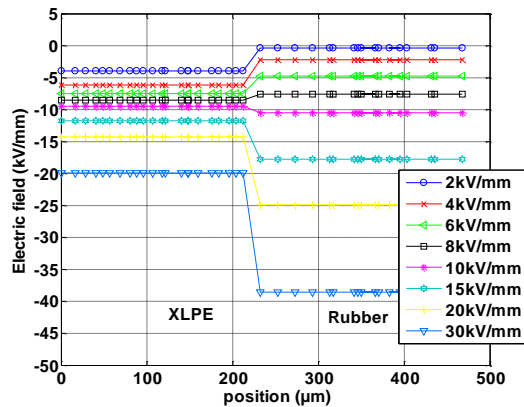


**Figure 12.** Electric field distributions in XLPE/rubber calculated by simulation at 40 °C under various electric fields.

A promising aspect of the above results is that, provided an appropriate characterization of the conductivity of constituting materials is achieved, a good estimate of the electric stress distribution in multilayer dielectrics can be reached. This is true regarding the sign of the interface charge, its build-up kinetics and the behavior upon polarity reversal which could be favorably compared considering modeling data issued from conductivity estimation and charge profiles by PEA measurements. With using an equation fitting both the low field and high field regime, it was possible to estimate interface charge density in a broad field range, including the discharge step where the field corresponds to the residual field due to the interface charge (not shown here). Bodega et al [2, 15-17] used an equation of conductivity of the form:

$$\sigma(T, E) \sim E^{\alpha_E} \cdot \exp(\alpha_T T). \quad (14)$$

with  $\alpha_E=1.8$  and  $\alpha_T=0.15 \text{ K}^{-1}$  to compute electric field distribution in different configurations of XLPE-EPR bilayer, including dual dielectrics in cylindrical geometry under temperature gradient [15, 17]. As the equation is in principle characteristic of the high field range (above a temperature dependent threshold field), its use should be limited to the validity range. Experimental field profiles and space charge profiles were reasonably well reproduced by the models under average fields of the order of 20 kV/mm.

The exercise of comparing space charge results and a model based on conductivity measurements only had some possibility to fail, as the techniques applied are different and the samples were not processed at the same place. It is to note that the nature of electrodes is the same: conductivity values and space charge profiles were both obtained on gold metalized samples. The results could be different with using different kinds of electrodes. Regarding the impact of the nature of electrode on conductivity, we did not realize measurements with different electrodes. As measurements on XLPE are relatively well documented, we have compared results of Bodega et al [2, 17], carried out using semiconducting electrodes, where results for different temperatures are reported, to the present results. The threshold field for non-linearity and the order of magnitude of the measured currents are similar. The conductivity seems to be more temperature-dependent in [17]; however there is no

definitive proof that it is related to the nature of the electrodes.

Actually, there are some evident deviations between model and experiments. One of them is of instrumental nature: Field distribution at the dielectric/dielectric interface is sharper in the model as compared to experiments. The true situation is probably in-between the two approaches: on the one hand the experimental field profiles are smoothed by the spatial resolution of the charge profile measurement method (the width at mid peak height is estimated to about 30  $\mu\text{m}$  at the interface in the present experiments); on the other hand, the hypothesis of a surface charge representing the MWS effect is rigorously wrong: accumulating charges are real charges moving through the sample. The spatial extension of the interface charge region should be controlled by processes and related quantities encompassing diffusion coefficient, mobility, trap density, and so on. So, accurate characterization of these interfacial charge phenomena requires on the one hand charge measurements methods providing excellent spatial resolution even in the bulk of the materials, and the development of transport models more refined than the conductivity approximation, on the other hand.

The other reason for deviation from experiments to model results is related to space charge accumulation in the material. Indeed, space charge measurements reveal also the presence of accumulated space charge within the bulk of both materials. At 40  $^{\circ}\text{C}$ , homocharges build up adjacent to both electrodes due to charges injection which seems to be more efficient with the increasing electric stress (cf. Figure 9b). At 70  $^{\circ}\text{C}$ , heterocharges accumulate adjacent to the cathode. Such a feature is often encountered in un-degassed XLPE material and is attributed to the dissociation of ionic species introduced by the various cross-linking by-products (e.g. acetophenone, cumyl alcohol, alpha-methyl-styrene for peroxide crosslinking).

The consequences of the build-up of these space charge is, on the one hand, a non-homogeneous field distribution in the dielectric layers, particularly in XLPE, and an underestimation of the maximum field in the insulation. One way of exploiting space charge measurement data for HVDC materials quality evaluation consists in measuring the field enhancement factor (FEF), more specifically the maximum FEF in space and time that may occur in a given geometry and for a given stressing protocol [18]. In the data of Figure 11 it can be deduced that the FEF exceeds 1.5 at 40  $^{\circ}\text{C}$  (maximum field divided by average field of 30 kV/mm in the bi-layer). Similar trends with an underestimation of the FEF brought by conduction model have been reported by Bodega [2] in the case of coaxial bi-layer structures constituting models for MV cables junctions.

Researches accompanying the development and the improvement of insulating materials for HVDC cables and accessories will require data collection on the field, time and temperature dependencies of conductivity and their use in engineering tools of field estimation. But, as targeted service fields are clearly in a non-linear conduction regime of materials, space charge measurement methods are to be used in conjunction with these field estimations, targeting on localization of regions of high FEF. This requires a good spatial resolution of the methods in the insulation bulk. The

improvement in model prediction will require the implementation of injection and transport models (treating conductivity through the true processes that are mobility and carrier production). A further interesting fact is that transport models are capable of predicting the localization of the so-called interface charge in the dielectric: again, as treated in the MWS approach, the volume density of interfacial charge is infinite, which is actually not physically sound.

## CONCLUSIONS

Expressions of conductivity versus temperature and electric field have been established using functional fitting of data from conduction current measurements carried out at various temperatures and electric stresses. Change in the apparent conduction regime with the electric field in addition to the temperature dependence of conductivity is taken into account in such expressions. Using the expressions of conductivity, the polarity of interfacial charge in bi-layer dielectric has been predicted for a range of temperature and applied fields applying the MW theory.

A deconvolution algorithm has been specifically developed to recover space charge profiles in bi-layer dielectrics taking into account the difference in acoustic and dielectric properties of the two materials. The temperature and the electric field dependences of the polarity and the density of interfacial charge have been highlighted through space charge measurements. Further, at any temperatures from 20 to 70  $^{\circ}\text{C}$  and at any field from 2 to 30 kV/mm, results regarding the sign of interfacial charges obtained from PEA measurements are in fair agreement with the theoretical MW interfacial charge which takes place when combining two materials having different permittivity and conductivity. The electric field distributions in bi-layer are derived from integration over position of space charge profiles. The highest electric stress is changing from XLPE to rubber material for electric field enabling the appearance of negative interface charge. This is in-line with simulation results.

## ACKNOWLEDGMENT

We are indebted to SilecCable for provision of materials and support of part of this study.

## REFERENCES

- [1] G. Mazzanti and M. Marzinotto, *Extruded Cables for High-Voltage Direct-Current Transmission*, Wiley-IEEE Press. New Jersey, 2013.
- [2] R. Bodega, *Space charge accumulation in polymeric high Voltage DC Cable systems*, Ph.D. degree Thesis, Delft University of Technology, 2006.
- [3] S. Delpino, D. Fabiani, G. C. Montanari, C. Laurent, G. Teyssedre, P. H. F. Morshuis, R. Bodega, and L. A. Dissado, "Polymeric HVDC Cable Design and Space Charge Accumulation. Part 2: Insulation Interfaces", *IEEE Electr. Insul. Mag.*, Vol. 24, No. 1, pp. 14-24, 2008.
- [4] M. Huang, Y. Zhou, Q. Sun, Y. Sha, and L. Zhang, "Effect of interface on space charge behavior in Multi-layer Oil-Paper insulation", *IEEE Conf. Electr. Insul. Dielectr. Phenomena*, pp. 654-657, 2012.

- [5] T. Takada, O. Kisanuki, M. Sakata, and M. Uchiumi, "Characteristics of space charge formed in a laminated LDPE/EVA dielectric under DC stress", IEEE Int'l. Sympos. Electr. Insul., pp. 184-187, 1996.
- [6] G.C. Montanari and P.H.F. Morshuis, "Space charge Phenomenology in Polymeric Insulating Materials", IEEE Trans. Dielectr. Electr. Insul., Vol. 12, pp. 754-767, 2005.
- [7] G.C. Montanari, I. Ghinello, F. Peruzzotti, and M. Albertini, "Behavior of Voltage-Current Characteristics and Threshold Indications for XLPE-Based Materials", IEEE Conf. Electr. Insul. Dielectr. Phenomena, pp. 128-131, 1998.
- [8] G.C. Montanari, "The electrical degradation threshold investigated by space charge and conduction current measurements", IEEE Trans. Dielectr. Electr. Insul., Vol. 7, pp. 309-315, 2000.
- [9] L.A. Dissado, C. Laurent, G.C. Montanari, P.H.F. Morshuis, "Demonstrating a threshold for trapped space charge accumulation in solid dielectrics under DC field," IEEE Trans. Dielectr. Electr. Insul., Vol. 12, pp. 612-620, 2005.
- [10] M. Nodat, L. Chow, and K.C. Kao, "Sublinear and superlinear current-voltage characteristics of amorphous  $Se_{1-x}Te_x$  films", J. Phys. D: Appl. Phys., Vol. 12, pp. 1345-1355, 1979.
- [11] S. Theoleyre and R. Tobazeon, "Ion injection by metallic electrodes in highly polar liquids of controlled conductivity", IEEE Trans. Electr. Insul., Vol. 20, pp. 213-220, 1985.
- [12] W. Choo, G. Chen, and S. G. Swingler, "Electric Field in Polymeric Cable due to Space Charge Accumulation under DC and Temperature Gradient", IEEE Trans. Dielectr. Electr. Insul., Vol. 18, pp. 596-606, 2011.
- [13] S. Boggs, H. Dwight, J. Hjerrild, J. T. Holbol, and M. Henriksen, "Effect of Insulation Properties on the Field Grading of Solid Dielectric DC Cable", IEEE Trans. Power Deliv., Vol. 16, pp. 456-462, 2001.
- [14] S. Qin and S. Boggs, "Design considerations for High Voltage DC components", IEEE Electr. Insul. Mag., Vol. 28, No. 6, pp. 36-44, 2012.
- [15] P.H.F. Morshuis, R. Bodega, D. Fabiani, G.C. Montanari, L.A. Dissado, and J.J. Smit, "Dielectric Interfaces in DC Constructions: Space Charge and Polarization Phenomena", IEEE Int'l. Conf. Solid Dielectr., pp. 450-453, 2007.
- [16] R. Bodega, P.H.F. Morshuis, U.H. Nilsson, G. Perego and J.J. Smit, "Polarization mechanisms of flat XLPE-EPR interfaces", Proc. Nord. Insul. Sympos., pp. 224-227, 2005.
- [17] P.H.F. Morshuis, R. Bodega, L.A. Dissado, C. Laurent, G.C. Montanari, U.H. Nilsson, G. Perego and G.C. Stevens, "Strategy and Tools for The Assessment of Polymeric Materials for HVDC Cable Systems", Proc. Cigré, D1-304, pp. 1-8, 2006.
- [18] B. Vissouvanadin, G. Teyssedre, S. Le Roy, C. Laurent, I. Denizet, M. Mammeri, and B. Poisson, "A methodology for the assessment of HVDC-XLPE cable insulation", 8th Int'l. Conf. Insul. Power Cable, Vol. 2, pp. 50-55, 2011.



**Thi Thu Nga Vu** was born in September 1981 in Hanoi, Vietnam. She received the Diploma in electrical engineering in 2004 and the Master's degree in 2007 from the Hanoi University of Science and Technology, in Vietnam. She has been working since 2004 as a researcher and lecturer at the Electric Power University in Hanoi, Vietnam. She received the Ph.D. degree in electrical engineering from the University of Toulouse in July 2014 for a research work on space charge accumulation and related phenomena in polymeric

insulating materials intended for HVDC cable application at the Laboratory of Plasma and Energy Conversion (LAPLACE) in Toulouse, France



**Gilbert Teyssedre** was born in May 1966 in Rodez, France. He received his Engineer degree in materials physics and graduated in solid state physics in 1989 at the National Institute for Applied Science (INSA). Then he joined the Solid State Physics Lab in Toulouse and obtained the Ph.D. degree in 1993 for work on ferroelectric polymers. He entered the CNRS in 1995 and has been working since then at the Electrical Engineering Lab (now LAPLACE) in Toulouse.

His research activities concern the development of luminescence techniques in insulating polymers with focus on chemical and physical structure, degradation phenomena, space charge and transport properties. He is currently Research Director at CNRS and is leading a team working on the reliability of dielectrics in electrical equipment.



**Bertrand Vissouvanadin** was born in Port-Bergé Madagascar, in September 1982. He received the Diploma in physics engineering from the National Institute of Applied Sciences, Toulouse, France, in 2007. He received the Ph.D. degree in electrical engineering from the University of Toulouse in 2011 for his work on synthetic materials for HVDC cables. He studied the electrical properties of radiation-cured epoxy during his post-doc at the Laboratory of Plasma and Energy Conversion (LAPLACE) in Toulouse. He is now working at

Liebherr-Aerospace in Toulouse and takes part in the development of electrical air conditioning systems for the next generation of aircraft.



**Séverine Le Roy** was born on 30 August 1977 in Belfort, France. She graduated in molecular and structural physical chemistry in 2001 at the Joseph Fourier University, Grenoble, France. Then she joined the Electrical Engineering Laboratory in Toulouse and obtained her Ph.D. degree in electrical engineering in 2004 from Paul Sabatier University. She entered the CNRS (National Centre of Scientific Research) in 2006. She is now dealing with modelling activities in relation with charge transport and ageing, for various domains of applications like electrical engineering, spatial environment. She is also concerned in the relationship between experiments and simulations.



**Christian Laurent** (M'98-SM'07) was born in Limoges, France, in 1953. He studied solid state physics at the National Institute for Applied Sciences in Toulouse and received his Eng. degree in physics in 1976. He joined the Electrical Engineering Laboratory at Paul Sabatier University in 1977 to study electrical treeing and partial discharge phenomena, which were the topics of his Dr. Eng. degree (1979). He joined CNRS (National Centre for Scientific Research) in 1981 and got his Doc-ès Sc. Phys. in 1984. In

1985, he spent one year as a post-doctoral fellow with the IBM "Almaden Research Center" where he studied plasma-polymerized thin films. Back in Toulouse he developed an approach to electrical ageing in polymeric materials based on luminescence analysis. He is now dealing with experimental and modeling activity relating to charge transport and ageing. He is currently Research Director at CNRS and Director of the Laboratory of Plasma and Energy Conversion -LAPLACE- in Toulouse.